Editors' Suggestion

Droplets sliding on single and multiple vertical fibers

M. Leonard [⦿],[1] J. Van Hulle,[1] F. Weyer [⦿],[1] D. Terwagne [⦿],[2] and N. Vandewalle[1]
[1]*GRASP, Physics Department, University de Liège, Belgium*
[2]*Frugal LAB, Physics Department, Université Libre de Bruxelles, Belgium*

From microfluidics to fog-harvesting applications, tiny droplets are transported along various solid substrates including hairs, threads, grooves, and other light structures. Driven by gravity, a droplet sliding along a vertical fiber is a complex problem since it is losing volume and speed as it goes down. With the help of an original setup, we solve this problem by tracking in real-time droplet characteristics and dynamics. Single fibers as well as multiple fiber systems are studied to consider the presence of grooves. On both fibers and grooved threads, droplet speed and volume are seen to decay rapidly because the liquid entity is leaving a thin film behind. This film exerts a capillary force able to stop the droplet motion before it is completely drained. A model is proposed to capture the droplet dynamics. We evidence also that multiple vertical fibers are enhancing the droplet speed while simultaneously promoting increased liquid loss on grooves.

I. INTRODUCTION

In arid or semiarid regions, the evolution of diverse flora and fauna has resulted in various survival strategies to access water despite the challenging conditions. Many of these living organisms utilize naturally occurring atmospheric water, either through fog collection [1–4] or promoting condensation [5]. Once collected, water must be transported to the area where the organism can absorb it. To achieve this, nature primarily relies on three fundamental principles: gravity [6], specific geometries, and wettability gradients [7], often in combination. In particular, specific geometries like conical shapes [5,8,9] or surfaces with specifically arranged substructures, such as grooves [8] and crevices [10], generate capillary forces.

If we consider gravity-driven transport, the dynamics of drops on vertical or inclined fibers is a complex phenomenon [11]. Indeed, depending on the inclination fiber angle [12], the fiber diameter [13], and the surface tension [14], the droplet may adopt two different shapes, barrel or clam, having different contact lines and therefore different dissipation mechanisms. The crossing of fibers has also been extensively studied from both a static [15,16] and a dynamic [17] view point. Notably, it has been shown in the dynamic case that a fiber crossing can stop or divide the droplet into small volumes [17]. The geometry of the crossing is the major parameter for determining the maximum volume remaining there [18,19]. A fiber array with selected fiber diameters is able to control the path of droplets [20]. When placing different immiscible liquids on a fiber array, multiple component droplets can be created, opening ways to microfluidic reactors and devices for probing biochemical reactions inside droplets. Several works have also proposed water harvesting using nets [21] or harps [22–24] which are constituted by vertical fibers transporting the droplets to a reservoir thanks to gravity. The dynamics of droplets sliding on fibers is therefore a key element for many applications from microfluidics to fog-harvesting devices.

To enhance transport efficiency, nature frequently arranges itself into multiple levels of structures. For instance, on the spines of a cactus, there are grooves, hairs, and spikes [5], while spider webs
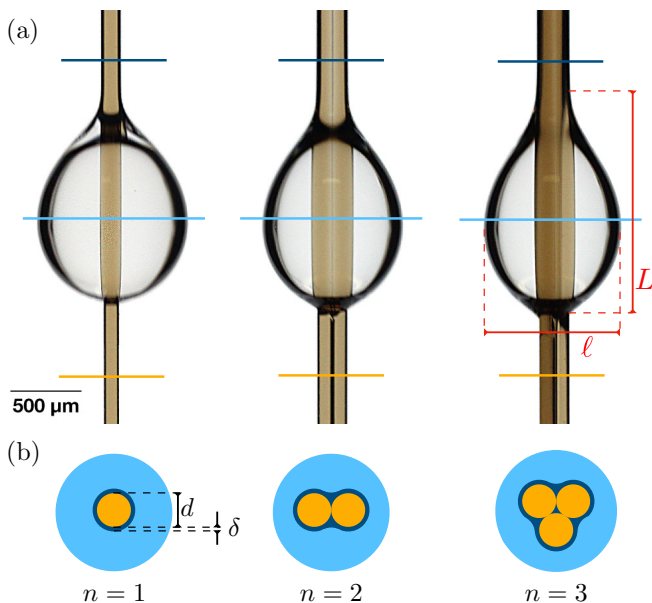
FIG. 1. (a) Experimental pictures of droplets of 3 µl sliding down one, two, and three fibers of $d = 140$ µm from left to right. A liquid film is seen behind the droplet. Droplet shape characteristics: the height L and the width ℓ are emphasized in red. (b) Sketch of three horizontal cuts of the system: dry fibers in front of the droplet (orange), the droplet cross section (light blue), and the liquid film of thickness δ after the passage of the droplet (dark blue).

feature silk beads [25]. These characteristics passively facilitate liquid transport through capillary driving forces [26,27].

To add some texture to the vertical fibers, we consider a bundle of fibers with grooves by assembling several fibers together, as shown in Fig. 1(a). This figure shows pictures of droplets sliding on $n = 1$, 2, and 3 adjacent vertical fibers of 140 µm in diameter. One observes that the shape of each droplet is significantly different at the bottom and top: while the fiber is dry before the passage of the droplet, a liquid film is left behind. The coating of the fiber is well seen in Fig. 1(a) and is sketched in Fig. 1(b). The presence of this liquid film explains partially the difference of local curvatures at the front and at the rear of the droplet. Because of the contact between the different fibers, grooves are formed and more liquid is expected to accumulate within. This may also change the droplet shape as seen depending on the number n of fibers in Fig. 1.

A fundamental question, which we address in the present paper, is to estimate the impact of these substructures on the droplet speed and liquid coating. This study represents a challenge since multiple physical characteristics of the droplet such as speed and volume should be measured synchronously. Thanks to the setup detailed below, we overcome this experimental difficulty, allowing for the modeling of moving droplets on fibers.

II. MATERIAL AND METHODS

Nylon fibers are used with diameters ranging from $d = 80$ µm to $d = 280$ µm. Bundles from $n = 1$ to $n = 4$ fibers were fabricated. Larger n values have been tested but the entire thread becomes so large that droplets lose their axisymmetric shape as described by Gabbard and Bostwick [14,28]. To guarantee fiber-to-fiber contact within the bundles, a slight torsion is applied, with a wavelength significantly larger than the droplet size. This ensures that the torsion does not interfere with the behavior of the droplets. By varying the number $n \leqslant 4$ of fibers, we modify the substructure of

TABLE I. Main characteristics of fiber bundles considered herein: effective diameter d_e and groove number n_g as a function of the number of fibers n.

Sketch	n	d_e	n_g
⬤	1	d	0
⬤⬤	2	$2d$	2
⬤⬤/⬤	3	$5d/2$	3
(cluster of 4)	4	$3d$	4
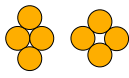
the vertical threads, forming n_g grooves. Please note that different configurations may form when n increases. In particular, for $n = 4$, two configurations can be formed but they possess similar characteristics. The effective diameter d_e of the structure is considered by comparing the external perimeter of the grooved structure with an equivalent cylinder. Table I summarizes the equivalent diameter d_e and the groove number n_g for the structures studied herein.

On these fibers and fiber bundles, we placed 3-μl-volume droplets, thanks to a micropipet. We chose silicone oils to ensure the total wetting of the fibers. However, changing n will modify the wetting conditions as observed in Fig. 1. The oil viscosity is in the range $\eta = 10^{-2}$ to 5×10^{-2} Pa s, its density is $\rho = 940$ kg/m^3, and its surface tension at 25 °C is 20×10^{-3} N/m.

Experiments are performed with the help of an original setup sketched in Fig. 2(a). The equipment considers a motorized fiber with an upward vertical motion in order to compensate the natural downward droplet motion. The experimental setup consists of two coils that are motorized and synchronized. Their purpose is to unwind the fiber from the lower coil to the upper one. Additionally, two external pulleys, which are held in place by springs, are used to maintain a tension in the fiber. The fiber itself is lighted from the back and the motion of the droplets is recorded from the front thanks to a charge-coupled device camera. The latter is connected to a computer which tracks the droplet in real time. A feedback loop adjusts the rotational speed of the spool motor to the droplet speed in order to keep the droplet at the center of the images. The speed v of the droplet is therefore measured. A sufficient length of wire (approximately 3 m) is wrapped around the lower coil. This allows for multiple experiments to be conducted before needing to rewind the wire in the opposite direction while cleaning the fiber with a tissue imbibed with isopropanol.

Moreover, the contour of the droplet is detected on each image. Thanks to Pappus's centroid theorem [29], the volume Ω of the droplet is estimated by integration, (i) assuming that the droplet keeps an axis symmetry around the fibers and (ii) by taking into account the volume of the portion of the fibers wrapped by the droplet. This method for measuring the volume is very good for single fibers; however, it becomes less reliable when droplet sizes become of the order of the bundle size. The shape characteristics of the droplet are also identified in the pictures: height L and width ℓ. Those lengths are sketched in Fig. 1(a). Typical data of synchronous measurement of the speed v and the volume Ω are shown in Fig. 2(b). One observes a fast decrease of both quantities over time.

The motion of the droplet along a single fiber or the bundle of fibers is driven by gravity and surface tension as revealed by the following nondimensional numbers. We can estimate the Bond number Bo $= \rho g \Omega / 2 \pi \gamma d_e$, which compares gravitational and capillary effects by taking the typical values of Ω in our experiments. We obtain Bo values around 0.75 for moving droplets, meaning that gravity drives the system, as well as capillary effects. The capillary number Ca $= v \eta / \gamma$ compares surface-tension effects to viscous ones. We have Ca values between 0.05 and 0.25, revealing that surface tension may overcome viscosity. The Weber number We $= \rho v^2 d_e / 8 \gamma$ is typically around 10^{-6} such that inertia can be neglected in the present study. This assumption has been considered in Ref. [12] where similar fiber sizes and drop volumes are considered.
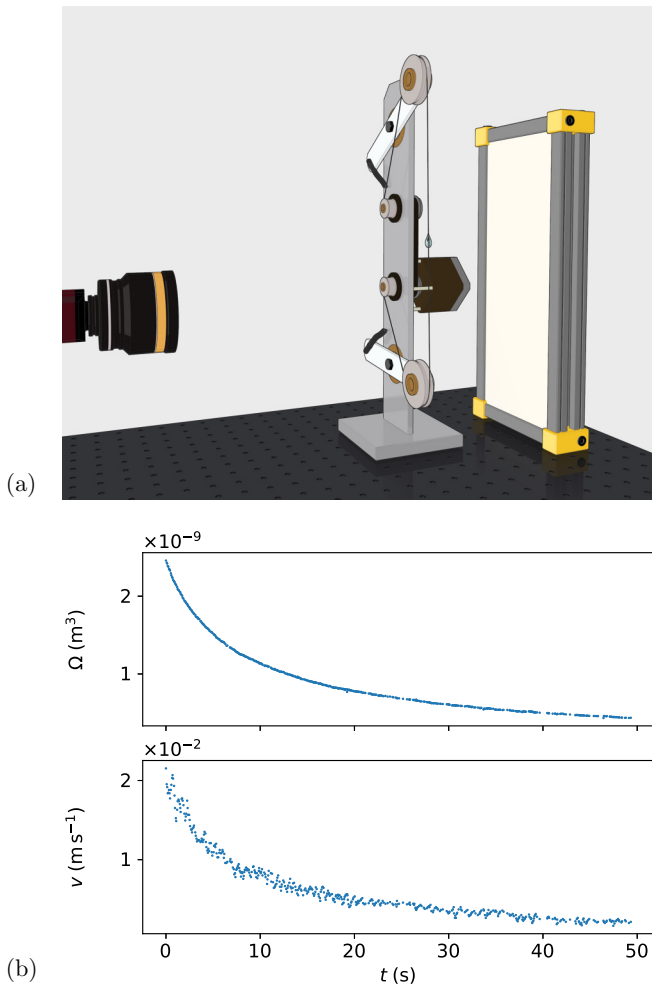
FIG. 2. (a) Sketch of the experimental setup where a camera records the droplet placed on a moving thread. Back illumination allows contrasted images. (b) Typical measurements of a droplet sliding on a single vertical fiber ($d = 140$ μm): both the volume Ω and the speed v are decreasing rapidly over time.

III. EXPERIMENTAL RESULTS

In the following, we present results with three different viscosities and for $n = 1$ to $n = 4$ using the same color code for all figures. From low to high viscosities, data are colored in green, blue, and red. From dark colors to light ones, the number of fibers is increased from $n = 1$ to $n = 4$. For each set of parameters, data are averaged over three to five experiments.

A. Droplet shape

Figure 3(a) shows the width ℓ and the height L of droplets over all experiments in a single plot. Color codes correspond to various $n = \{1, 2, 3, 4\}$ values and various viscosities $\eta = \{10^{-2}, 2 \times 10^{-2}, 5 \times 10^{-2}\}$ Pa s. Since the droplet volume $\Omega \approx \pi \ell^2 L/6 - \pi d_e^2 L/4$ is decreasing during the experiments, geometrical characteristics ℓ and L are evolving and are plotted in this figure. A linear behavior is found for each set of data points. The slope is close to unity meaning that droplet characteristic lengths are evolving in a similar way. There is, however, an offset which
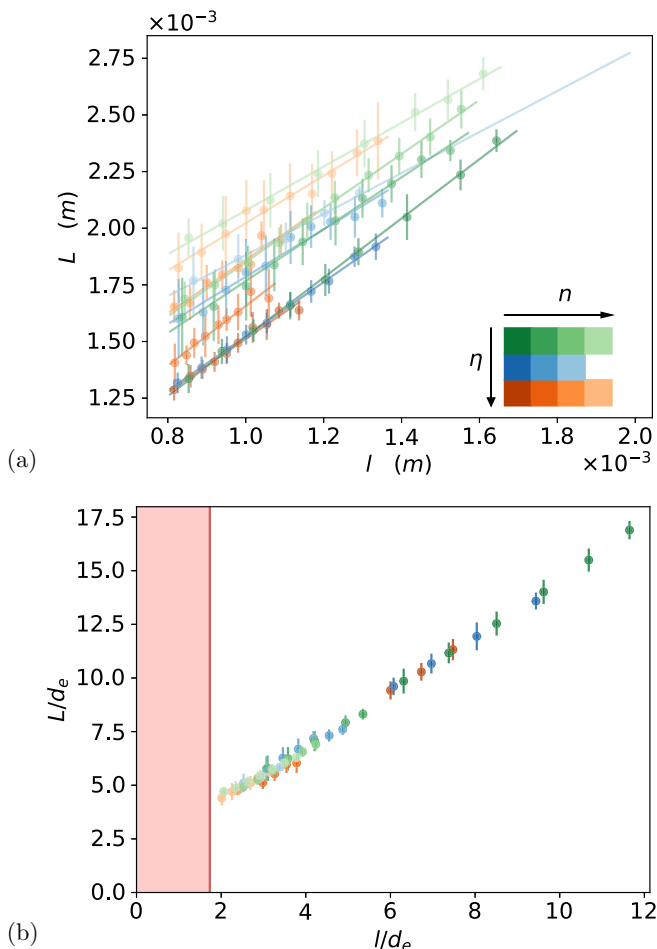
FIG. 3. (a) Height of the droplet L as a function of the width ℓ of the droplet. All data points are colored as a function of the viscosity η and the fiber number n. See the color legend given as an inset. (b) Lengths are rescaled by the effective diameter d_e. The region colored in red corresponds to the $\Omega_c < 1$ criterion, such that a droplet there is no longer in a barrel configuration.

depends roughly on the fiber number n. The droplets seem more elongated when grooves are present. The spreading of a droplet is indeed enhanced on grooved substrates, as studied recently in Ref. [27].

By normalizing ℓ and L by the effective thread diameter d_e, all data points collapse around a single linear behavior in Fig. 3(b). This finding implies that d_e is a pertinent parameter for characterizing both the shape and the size of droplets, regardless of viscosity or fiber count. Furthermore, the collapse of the data highlights the fact that the number of grooves does not affect the geometry of the droplets. It should be remarked that droplets on fibers are often considered in the scientific literature as nearly spherical objects [12,30,31] with an aspect ratio close to unity. We, however, evidence herein aspect ratios in the range $L/\ell \approx 1.4$–1.8 in dynamical cases.

The red-colored region in Fig. 3(b) at small ℓ/d_e values is where droplets should leave their barrel shape to become a clam shape. Indeed, it is possible to define the reduced volume, denoted by Ω_c, which represents the ratio of the droplet's volume Ω to the volume of the fiber $\pi d_e^2 L/4$ enclosed by the droplet. The criterion for keeping a barrel shape droplet is given by $\Omega_c > 1$ [9,30]. Taking the

characteristic lengths into account, this barrel shape criterion becomes

$$\frac{\ell}{d_e} > \sqrt{3}, \tag{1}$$

where all our data are seen. The lower limit $\ell = \sqrt{3}d_e$ is denoted by a red vertical line in Fig. 3(b).

B. Film thickness

The volume Ω is decreasing as the droplet slides along the fiber, leaving a thin film behind. Liquid volume conservation states that

$$\dot{\Omega} = -\pi d_e \delta v, \tag{2}$$

where $\delta \ll d_e$ is the thickness of the liquid film left behind the droplet, as observed and sketched in Fig. 1. Whatever the η and n values, a nearly linear behavior is obtained in Fig. 4(a) when $\dot{\Omega}$ is plotted as a function of the speed v. All results are shown following the same color code as the inset of Fig. 3. Different slopes are observed, depending on the viscosity η and the number n of fibers.

From the slopes measured in Fig. 4(a), the relationship in Eq. (2) allows us to estimate the average film thickness $\bar{\delta}$ left behind droplets. Results are plotted in Fig. 4(b) as a function of n. Typical values for $\bar{\delta}$ range from 10 to 50 μm. The film thickness is seen to be highly dependent on the liquid viscosity η. It should also be remarked that the presence of grooves ($n > 1$) has also an important effect on the film thickness. Indeed, a clear increase of $\bar{\delta}$ is observed for all viscosities in Fig. 4(b). In fact, liquid amounts are accumulated into the grooves. The above behaviors are emphasized in Fig. 4(b) by colored lines which are guides for the eye.

Moreover, the Landau-Levich model [32] of liquid coating is predicting a film thickness $\delta \propto \mathrm{Ca}^{2/3}$, and more precisely,

$$\delta = 0.67 d_e \left(\frac{\eta v}{\gamma}\right)^{2/3} \tag{3}$$

as proposed in Ref. [33]. The volume loss vs speed should therefore scale as $\dot{\Omega} \propto -v^{5/3}$. However, the range of speed values (or Ca values) is less than a decade, such that a nearly linear behavior is observed in Fig. 4(a) instead. Higher speeds cannot be reached with this experimental setup. Nevertheless, the liquid coating is highly sensitive to viscosity, and one expects that the film thickness increases as $\bar{\delta} \propto \eta^{2/3}$. For a single fiber ($n = 1$), the three measured thicknesses are in agreement with the Landau-Levich model since $\bar{\delta}/\eta^{2/3}$ gives a unique value of 2.5×10^{-4} m/(Pa s)$^{2/3}$ within error bars, as observed in Fig. 4(c). The cases with grooves ($n > 1$) are different since the penetration of the liquid into grooves relies heavily on viscosity, and here the Landau-Levich model ceases to provide accurate predictions.

C. Droplet speed

In Fig. 5(a), the speed v of the droplet is plotted as a function of the measured volume Ω. One may notice that the speed increases with the volume, a result which is consistent since the weight of the droplet is the driving force of the problem. A linear behavior is observed between both physical quantities. Increasing the effective fiber diameter d_e reduces the speed and, more precisely, the slope of the linear behavior. Also, different oil viscosities have been used in order to evidence the role of dissipation mechanisms. Increasing the viscosity has an effect on the speed, which is reduced accordingly. On top of that observation, we can remark that all linear trends are converging towards a particular volume at zero speed. It means that below that particular volume Ω_0, tiny droplets are static on the vertical fiber. This particular volume seems more dependent on fiber diameter than on viscosity, as we will see below.
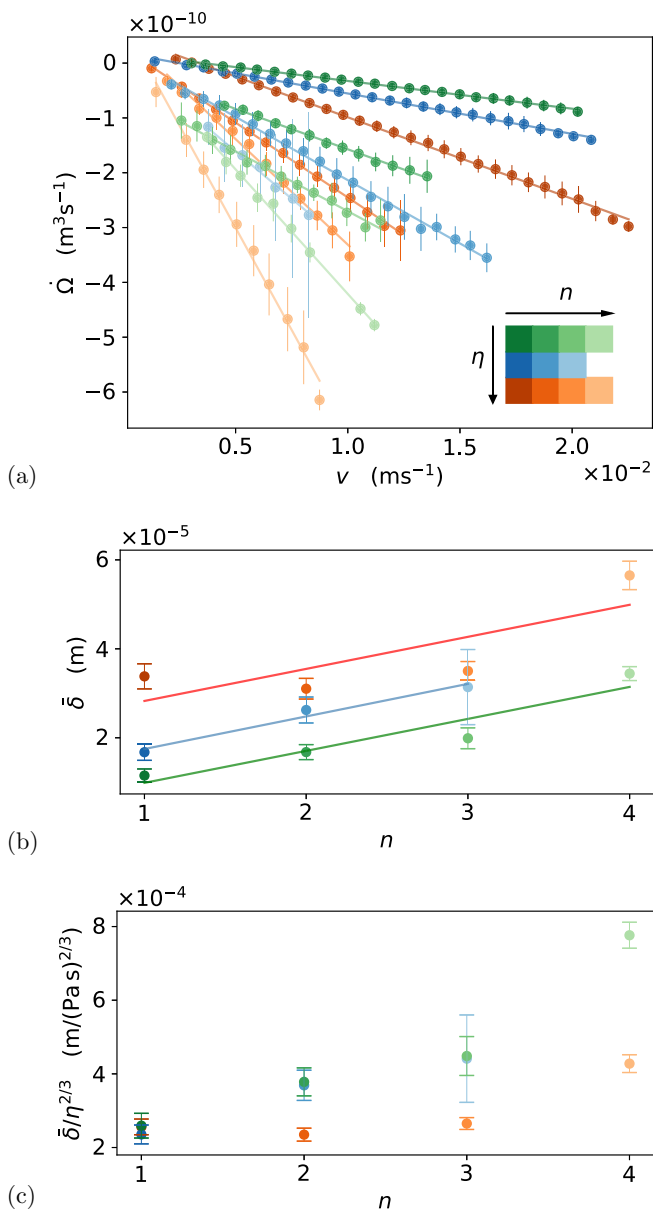
FIG. 4. (a) Volume loss rate $\dot{\Omega}$ as a function of the droplet speed v. Lines are linear fits used to extract the slopes for determining $\bar{\delta}$ from Eq. (2). (b) Average liquid film thickness $\bar{\delta}$ as a function of n. Lines are fitted on the data to emphasize η and n dependencies, but should be considered as guides for the eye. (c) Average film thickness normalized by $\eta^{2/3}$, emphasizing that the effect of viscosity is captured by the Landau-Levich model only for $n = 1$.

IV. DISCUSSION

A. Droplet dynamics

In order to capture the linear behaviors of Fig. 5(a), i.e., the droplet dynamics, we propose a model based on the sum of three forces acting on the droplet: gravity, dissipation, and capillary. The
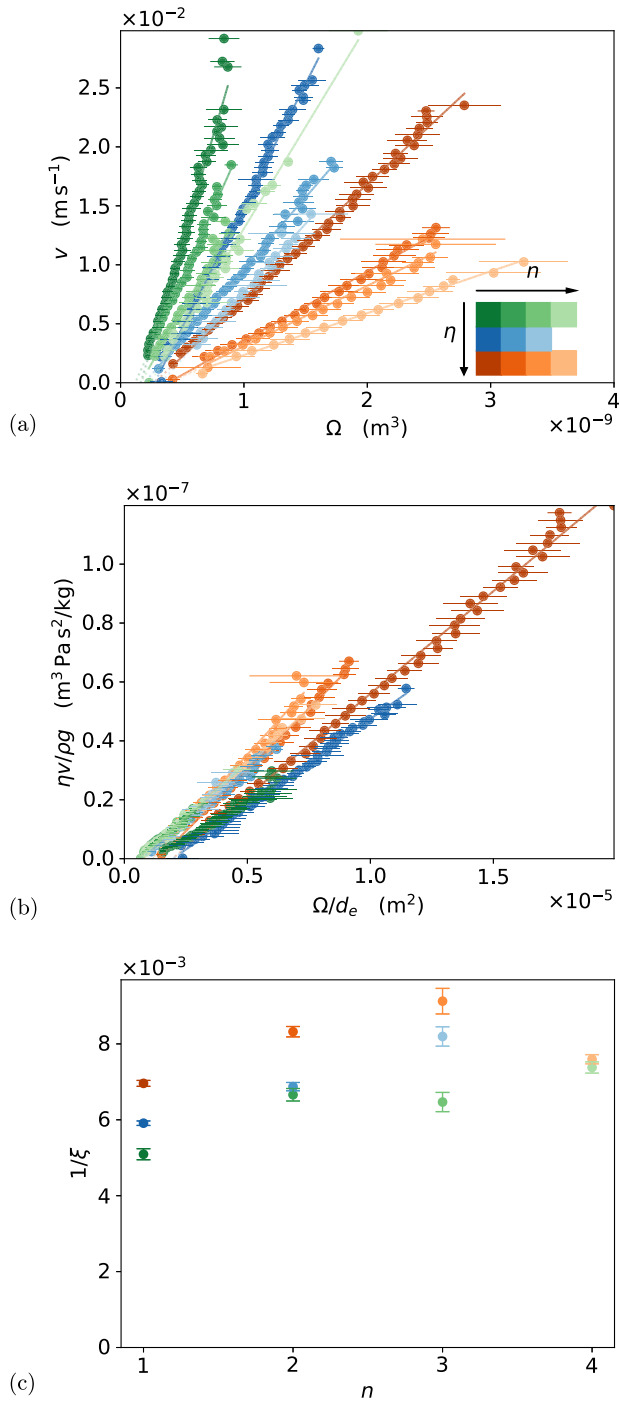
FIG. 5. (a) Droplet speed as a function of Ω emphasizing the gravity-driven mechanism. Each color is associated witht the viscosity η and the fiber number n. Error bars are given. Data are fitted by a linear model of Eq. (7). (b) Rescaled speed v and volume Ω according to Eq. (7). (c) From the slopes extracted in panel (a), the inverse dissipation factor $1/\xi$ is estimated. It is plotted as a function of n with the same color code. One observes that the presence of grooves favors the droplet motion; i.e., $1/\xi$ increases with n.

driving force is the weight of the droplet and is given by $F_g = \rho g \Omega$, where g is the gravitational acceleration.

Dissipation should play an important role, and following Ref. [12], we consider a classical drag force, $F_d = -\xi \eta d_e v$, where ξ is a dissipation factor. Assuming that the friction force F_d is mainly due to velocity gradients within the droplet, and following Ref. [12,31], one has

$$F_d = -\pi d_e \int_{a_f}^{L/2} c \frac{\eta v}{z} \frac{L}{\ell} dz + \pi d_e \int_{L/2}^{a_r} c \frac{\eta v}{z} \frac{L}{\ell} dz, \qquad (4)$$

where velocity gradients v/z are integrated from the shortest distance from the contact line at either the front a_f or the rear a_r of the droplet. We cut the droplet in equal parts $L/2$ despite the lack of front and rear symmetry, because the sources of dissipation are mainly located at the front and at the rear of the droplet. The dimensionless constant c is a geometrical factor close to unity studied in Ref. [12]. After integration over the front of the droplet and the rear of the droplet, the main contributions to ξ are due to the front and rear characteristics, and more precisely,

$$\xi = c\pi \frac{L}{\ell} \ln \left(\frac{L^2}{4 a_f a_r} \right). \qquad (5)$$

In front of the droplet, the fiber is dry such that a_f is estimated to be $a_f \approx 10^{-9}$ m from de Gennes [34] while at the rear of the droplet this distance is limited by the film thickness $a_r = \delta$. Injecting geometrical characteristics L/ℓ as measured herein and $\bar{\delta}$ around 10 μm, one obtains $\xi \approx 115$.

The capillary force is acting on both sides of the droplet. In the front, i.e., at the bottom of the droplet, the contact line separates a dry fiber and the droplet, such that the contribution to the capillary force is given by $\pi \gamma d_e$. Indeed, silicone oil is totally spreading on the fiber such that the contact angle can be considered as zero. Behind the droplet, the capillary force comes from the liquid film. One has the contribution $-\pi(d_e + \delta)\gamma$. Summing both contributions gives the capillary force $F_c = -\pi \delta \gamma$.

Therefore, taking into account for the sum of the forces acting on the droplet, the equation of motion becomes

$$\rho \Omega \dot{v} = \rho g \Omega - \pi \delta \gamma - \xi \eta d_e v. \qquad (6)$$

Neglecting inertia, as suggested at the end of Sec. II, the speed of the droplet v is given by

$$v = \frac{\rho g \Omega}{\xi \eta d_e} - \frac{\pi \gamma \delta}{\xi \eta d_e}. \qquad (7)$$

One finds the linear dependency of the speed with the droplet's volume with a single slope. Figure 5(b) plots normalized quantities $\eta v / \rho g$ as a function of Ω / d_e to evidence such linear behavior. Different slopes are, however, observed, indicating that the dissipation factor depends on η and n. This is discussed in the next subsection.

Setting the speed to zero in Eq. (7), one can find the volume offset Ω_0 as

$$\Omega_0 = \frac{\pi \delta \gamma}{\rho g}. \qquad (8)$$

Injecting the values of surface tension and density in the last relationship, one finds a typical volume offset around 0.1 μℓ, in agreement with our measurements. Please note that the above condition can be interpreted in terms of Bond numbers. Indeed, Eq. (8) can be rewritten as $\text{Bo}_c = \bar{\delta}/2d_e \approx 0.05$, meaning that all droplets characterized by a larger Bond number are moving until they lose volume and reach this critical low-Bo_c value.
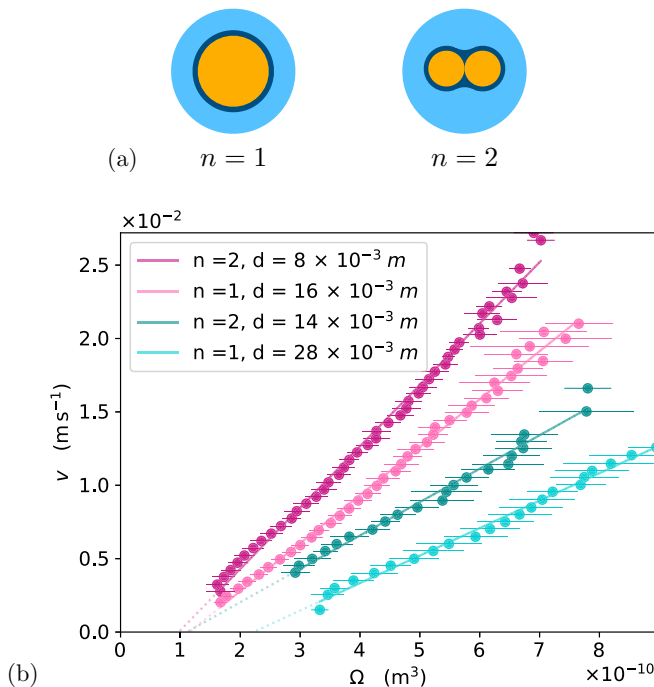
FIG. 6. (a) Sketch of the additional experiment where a single fiber of diameter d is compared with $n = 2$ fibers of diameter $d/2$. The equivalent diameter d_e is therefore conserved but grooves are present in the second case. (b) Droplet speed as a function of droplet volume for two situations illustrated in panel (a). Extra speed is clearly obtained for $n = 2$.

B. Dissipation factor

By fitting the slopes of Fig. 5(b) with Eq. (7), the inverse dissipation factor $1/\xi$ can be extracted from all experiments. The results are shown in Fig. 5(c). One observes that the dissipation factor (and therefore the droplet speed) is dependent on the viscosity η and the fiber number n. The values of $1/\xi$ are close to the one estimated in the previous subsection, i.e., $1/\xi \approx 1/115 = 8.7 \times 10^{-3}$. Surprisingly, the inverse dissipation factor seems more important for intermediate n values, such that higher speeds are observed for fiber bundles. The effect is already present for $n = 2$ and $n = 3$. There, a significant speed increase of about 20% is obtained from the single fiber case. This effect is counterintuitive.

In Fig. 5(c), one observes that ξ decreases with η and is quite sensitive to the substructure, i.e., depends on n. Indeed, Eq. (5) links ξ to δ. Since high viscosities imply thicker films behind the droplet, one expects less dissipation. A second observation is that substructure has a significant effect on dissipation since ξ is lower for $n = 2$ and $n = 3$ than for $n = 1$. Of course, the previous argument on film thickness could be also used. Grooves allow for faster droplet motion due to thicker films behind. It is hard to separate effects, but it should be noted that the groove effect is significant with 20% extra speeds for some configurations.

To assess the effect of grooves, we performed additional experiments. In Fig. 6, droplet dynamics are shown for comparing the case of a single fiber of diameter d with two adjacent fibers of diameter $d/2$, thus fixing the equivalent diameter $d_e = d$. Two different diameters d are tested. In both cases, the droplet speed v is much higher when $n = 2$ than when $n = 1$. These additional experiments confirm extra speed for two joined fibers equivalent to a single one.

A last remark is that the dynamics emphasized above leads to a more complex phenomenon on longer times. Indeed, any droplet is losing volume and finally stops when reaching Ω_0. After

a while, the coating left above the immobile mother droplet forms smaller daughter droplets due to the classical Rayleigh-Plateau instability. Those daughter droplets are on a prewetted fiber such that they start moving as soon as they grow. Finally they reach the mother droplet. Fed by daughter droplets, the mother droplet starts again its motion till reaching again Ω_0. A start and stop motion of the primary droplet develops. Future works will focus on this phenomenon.

V. CONCLUSION

In this paper, we built an experimental setup able to measure simultaneously droplet speed v and volume Ω during the droplets' motion on various threads. The dynamics of the droplet motion was captured and models were proposed. Such measurements allow for estimating the dissipation factor ξ, which is dependent on viscosity because of the film thickness left behind.

On top of that, we evidenced that the droplet motion is deeply affected by the substructure of the vertical thread. Indeed, grooves are collecting more liquid such that the film thickness left behind the droplet depends on the groove number. As a consequence, dissipation is modified such that extra speeds (up to 20%) are observed with threads possessing grooves rather than smooth cases.

The findings of this study have practical implications for water-harvesting applications, as droplet velocity along fibers has a direct impact on the efficiency of water capture. Vertical fiber-based structures, known as harps, have shown great potential in water harvesting [23] and efficiently drain water after a certain onset time [35]. The onset time refers to the time required for the first captured droplets to begin draining and is a primordial characteristic in weather-changing conditions. The use of fiber bundles, as described in this article, has the potential to reduce the onset time of these structures.

Another application concerns characterization methods. Indeed, our setup is able to extract relevant information about the dissipation inside droplets. The system can therefore be used as a type of rheometer. Such a device will be developed in the future and could be tested with other liquids like non-Newtonian and complex liquids.

ACKNOWLEDGMENT

[1] M. Ebner, T. Miranda, and A. Roth-Nebelsick, Efficient fog harvesting by *Stipagrostis sabulicola* (Namib dune bushman grass), J. Arid Environ. **75**, 524 (2011).

[2] H. Andrews, E. Eccles, W. Schofield, and J. Badyal, Three-dimensional hierarchical structures for fog harvesting, Langmuir **27**, 3798 (2011).

[3] Z. Pan, W. G. Pitt, Y. Zhang, N. Wu, Y. Tao, and T. T. Truscott, The upside-down water collection system of *Syntrichia caninervis*, Nat. Plants **2**, 16076 (2016).

[4] F. Ito, S. Komatsubara, N. Shigezawa, H. Morikawa, Y. Murakami, K. Yoshino, and S. Yamanaka, Mechanics of water collection in plants via morphology change of conical hairs, Appl. Phys. Lett. **106**, 133701 (2015).

[5] J. Ju, H. Bai, Y. Zheng, T. Zhao, R. Fang, and L. Jiang, A multi-structural and multi-functional integrated fog collection system in cactus, Nat. Commun. **3**, 1247 (2012).

[6] A. Roth-Nebelsick, M. Ebner, T. Miranda, V. Gottschalk, D. Voigt, S. Gorb, T. Stegmaier, J. Sarsour, M. Linke, and W. Konrad, Leaf surface structures enable the endemic Namib desert grass *Stipagrostis sabulicola* to irrigate itself with fog water, J. R. Soc. Interface. **9**, 1965 (2012).

[7] J. Guadarrama-Cetina, A. Mongruel, M. G. Medici, E. Baquero, A. R. Parker, I. Milimouk-Melnytchuk, W. González-Viñas, and D. Beysens, Dew condensation on desert beetle skin, Eur. Phys. J. E **37**, 109 (2014).

[8] H. Chen, T. Ran, Y. Gan, J. Zhou, Y. Zhang, L. Zhang, D. Zhang, and L. Jiang, Ultrafast water harvesting and transport in hierarchical microchannels, Nat. Mater. **17**, 935 (2018).

[9] J. Van Hulle, F. Weyer, S. Dorbolo, and N. Vandewalle, Capillary transport from barrel to clamshell droplets on conical fibers, Phys. Rev. Fluids **6**, 024501 (2021).

[10] Z. Shi, Z. Tang, B. Xu, L. Jiang, and H. Liu, Bioinspired directional liquid transport induced by the corner effect, Nano Res. **16**, 3913 (2023).

[11] Z. Huang, X. Liao, Y. Kang, G. Yin, and Y. Yao, Equilibrium of drops on inclined fibers, J. Colloid Interface Sci. **330**, 399 (2009).

[12] T. Gilet, D. Terwagne, and N. Vandewalle, Droplets sliding on fibres, Eur. Phys. J. E **31**, 253 (2010).

[13] G. McHale, M. I. Newton, and B. J. Carroll, The shape and stability of small liquid drops on fibers, Oil & Gas Sci. Technol. **56**, 47 (2001).

[14] C. T. Gabbard and J. B. Bostwick, Asymmetric instability in thin-film flow down a fiber, Phys. Rev. Fluids **6**, 034005 (2021).

[15] C. Duprat, S. Protiere, A. Beebe, and H. A. Stone, Wetting of flexible fibre arrays, Nature (London) **482**, 510 (2012).

[16] A. Sauret, F. Boulogne, D. Cébron, E. Dressaire, and H. A. Stone, Wetting morphologies on an array of fibers of different radii, Soft Matter **11**, 4034 (2015).

[17] T. Gilet, D. Terwagne, and N. Vandewalle, Digital microfluidics on a wire, Appl. Phys. Lett. **95**, 014106 (2009).

[18] F. Weyer, M. Lismont, L. Dreesen, and N. Vandewalle, Compound droplet manipulations on fiber arrays, Soft Matter **11**, 7086 (2015).

[19] Z. Pan, F. Weyer, W. G. Pitt, N. Vandewalle, and T. T. Truscott, Drop on a bent fibre, Soft Matter **14**, 3724 (2018).

[20] F. Weyer, A. Duchesne, and N. Vandewalle, Switching behavior of droplets crossing nodes on a fiber network, Sci. Rep. **7**, 13309 (2017).

[21] K.-C. Park, S. S. Chhatre, S. Srinivasan, R. E. Cohen, and G. H. McKinley, Optimal design of permeable fiber network structures for fog harvesting, Langmuir **29**, 13269 (2013).

[22] W. Shi, M. J. Anderson, J. B. Tulkoff, B. S. Kennedy, and J. B. Boreyko, Fog harvesting with harps, ACS Appl. Mater. Interfaces **10**, 11979 (2018).

[23] W. Shi, T. W. van der Sloot, B. J. Hart, B. S. Kennedy, and J. B. Boreyko, Harps enable water harvesting under light fog conditions, Adv. Sustainable Syst. **4**, 2000040 (2020).

[24] Y. Jiang, C. Machado, and K. K. Park, From capture to transport: A review of engineered surfaces for fog collection, Droplet **2**, e55 (2023).

[25] Y. Zheng, H. Bai, Z. Huang, X. Tian, F.-Q. Nie, Y. Zhao, J. Zhai, and L. Jiang, Directional water collection on wetted spider silk, Nature (London) **463**, 640 (2010).

[26] P. Kolliopoulos, K. S. Jochem, D. Johnson, W. J. Suszynski, L. F. Francis, and S. Kumar, Capillary-flow dynamics in open rectangular microchannels, J. Fluid Mech. **911**, A32 (2021).

[27] J. Van Hulle and N. Vandewalle, Effect of groove curvature on droplet spreading, Soft Matter **19**, 4669 (2023).

[28] C. T. Gabbard and J. B. Bostwick, Bead-on-fibre morphology in shear-thinning flow, J. Fluid Mech. **961**, A14 (2023).

[29] J. W.F.Kern, *Solid Mensuration with Proofs* (Wiley, New York, 1948).

[30] B. Carroll, Equilibrium conformations of liquid drops on thin cylinders under forces of capillarity: A theory for the roll-up process, Langmuir **2**, 248 (1986).

[31] E. Lorenceau and D. Quéré, Drops on a conical wire, J. Fluid Mech. **510**, 29 (2004).

[32] L. Landau and B. Levich, Dragging of a liquid by a moving plate, in *Dynamics of Curved Fronts*, edited by P. Pelcé (Academic Press, San Diego, 1988), pp. 141–153.

[33] D. Quéré, Fluid coating on a fiber, Annu. Rev. Fluid Mech. **31**, 347 (1999).

[34] P.-G. de Gennes, Wetting: statics and dynamics, Rev. Mod. Phys. **57**, 827 (1985).

[35] Y. Jiang, C. Machado, S. Savarirayan, N. A. Patankar, and K.-C. Park, Onset time of fog collection, Soft Matter **15**, 6779 (2019).